

Topological Effects of Noise on Nonlinear Dynamics

Gisela D. Charó,^{1,2,*} Mickaël D. Chekroun,^{3,4} Denisse Sciamarella,² and Michael Ghil^{3,5}

¹*Centro de Investigaciones del Mar y la Atmósfera, Facultad de Ciencias Exactas y Naturales, Universidad de Buenos Aires, C1428EGA CABA, Argentina.*

²*Institut Franco-Argentin d'Études sur le Climat et ses Impacts (IFAECI), UMI 3351 (CNRS-CONICET-UBA), C1428EGA CABA, Argentina.*

³*Department of Atmospheric & Oceanic Sciences, University of California, Los Angeles, CA 90095-1565, USA*

⁴*Weizmann Institute of Science, Rehovot, Israel.*

⁵*Geosciences Department and Laboratoire de Météorologie Dynamique (CNRS and IPSL), École Normale Supérieure and PSL University, 75231 Paris Cedex 05, France*

(Dated: December 31, 2022)

Noise modifies the behavior of chaotic systems. Algebraic topology sheds light on the most fundamental effects involved, as illustrated here by using the Lorenz (1963) model. This model's attractor is “strange” but frozen in time. When driven by multiplicative noise, the Lorenz model's random attractor (LORA) evolves in time. Here, we use Branched Manifold Analysis via Homologies (BraMAH) to describe LORA's coarse-grained branched manifold. BraMAH is thus extended from deterministic flows to noise-driven systems. LORA's homology groups change in time and differ from the deterministic one.

I. INTRODUCTION

The climate system has a complex and nonlinear behavior, its fundamental components — the atmosphere, oceans, and ice sheets — evolve on many different time and space scales [1, 2]. This unstable and dissipative system exhibits natural variability and is driven by external forcings [3, 4]. Physically open systems, modeled as nonautonomous dynamical systems, allow for deterministic (anthropogenic) as well as random (natural) forcing. The theory of nonautonomous (NDSs; [5]) and random (RDSs; [6]) dynamical systems provides appropriate mathematical settings to address truly coupled ocean-atmosphere behavior and climate change [7]. The interest in bifurcations in the climate system has gained attention since the introduction of the term tipping points [4, 8]. Tipping points generalize the bifurcation concept in open systems that are modeled by NDSs or RDSs [9].

In examples such as the ocean's wind-driven circulation, a certain degree of realism requires considering not only a stochastic time-dependent forcing but also relying on a model's probability density function (PDF) rather than on pointwise simulation alone. The study of RDSs and their time-dependent invariant measures μ_t , known as sample measures [10, 11], addresses these challenges [7, 12]; see Appendices A-C.

Algebraic topology [13] studies algebraic invariants that classify topological spaces up to homeomorphism [14]. Applications to deterministic dynamical systems are relatively recent and are also known as chaos topology [15–17]. Chaotic attractors can be classified by branched manifolds [18], following [19–21].

The question that inevitably arises about random attractors is: what is the effect of a stochastic perturbation

on a nonlinear system's topological structure? Chekroun et al. [12] have shown that the well-known smoothing effect of noise disappears in a pullback approach. When the unperturbed nonlinear system's dynamics is chaotic, the random pullback attractor is a time-dependent object that typically exhibits a fine structure of amazing complexity that is highlighted by its sample measure.

More precisely, random attractors reveal that fractal structures can survive the noise and be fed by it, as shown for the first time numerically in [12] for the stochastic Lorenz [22] model's (SLM's) random attractor. This striking property arises, in particular, when the stochastic system's generator is hypoelliptic and its leading Lyapunov exponent is positive [12].

This paper presents, as far as we know, the first application of Branched Manifold Analysis via Homologies (BraMAH) to nonlinear, chaotic systems driven by noise. In it, we show that the random attractor's structure is well represented, at each instant in time, by a branched manifold. The latter is defined here locally as an integer-dimensional subset of phase space that provides a robust skeleton of the point cloud associated with the sample measure; see Appendix C. This definition of a branched manifold is more general than the usual one in the purely deterministic context, where the invariant manifold is relative to a flow in phase space and defined through a Birman-Williams projection [18, 19].

The present work shows how the topological structure approximating LORA's instantaneous sample measure is seen through the lens provided by the homological description of its associated branched manifold. We study here changes in LORA's topology — i.e., topological tipping points — produced by the driving noise.

* gisela.charo@cima.fcen.uba.ar

II. METHOD

In the deterministic framework, the topological description of the branched manifold encodes the invariant structure of an attractor in phase space. Methods to extract a branched manifold's topology from time series have been respectively adapted by [16] and [23] to noisy data and to material lines in fluid flows.

Sciamarella and Mindlin [16, 17] formulated and tested the BraMAH method to extract the topological structure of chaotic flows from noisy time series. To do so, one embeds the time series in a suitable phase space and approximates the structure of the invariant manifold with “building blocks.” In algebraic topology, these blocks are Euclidean closed sets (segments, disks, etc.), called n -cells, where $n \in \mathbb{N}_0$. A point is a 0-cell, a line segment joining two points is a 1-cell, a polygon is a 2-cell and so forth. Once assembled, these cells form a “rough skeleton” of the branched manifold, called a cell complex.

The topological structure of this cell complex is studied by using a key tool of algebraic topology [24], namely homology groups H_n . These groups identify the nonequivalent k -dimensional holes (k -holes) of a topological space of dimension n , where $k \in \mathbb{N}_0$ and $k \leq n$. H_0 identifies the connected components (0-holes), H_1 the cycles (1-holes), H_2 the cavities (2-holes), and H_n the hypercavities (n -holes). BraMAH also computes the orientability chains of the cell complex, which provide information about the branched manifold's torsions, such as those in a Möbius strip or Klein bottle.

Recently, Topological Data Analysis (TDA) [25–27] has been widely used in machine learning to extract topology from data. TDA often relies on persistence homology, which monitors the “lifetime” of basic topological features, such as the n -holes, with respect to increases in a parameter used to construct a family of nested cell complexes. Persistence homology may also be used to describe an RDS but it is less informative than BraMAH, since it is basically a metric approach and does not aim to characterize a branched manifold.

When evaluating a time-dependent structure like LORA, one has to ask whether its topology is time-dependent. In order to answer this question, we will take two steps: (1) generate point clouds that approximate LORA at successive time instants, called “snapshots” [12, 28, 29]; and (2) compute the topological properties of these structures using BraMAH.

In the first step, the point cloud approximating LORA is generated by solutions of the SLM introduced in [12]. In SLM, the equations of the classical Lorenz [22] deterministic model are perturbed by a multiplicative noise in the Itô sense [6], with W_t a Wiener process and $\sigma > 0$ the noise intensity:

$$\begin{aligned} dx &= s(y - x)dt + \sigma x dW_t, \\ dy &= (rx - y - xz)dt + \sigma y dW_t, \\ dz &= (-bz + xy)dt + \sigma z dW_t; \end{aligned} \quad (1)$$

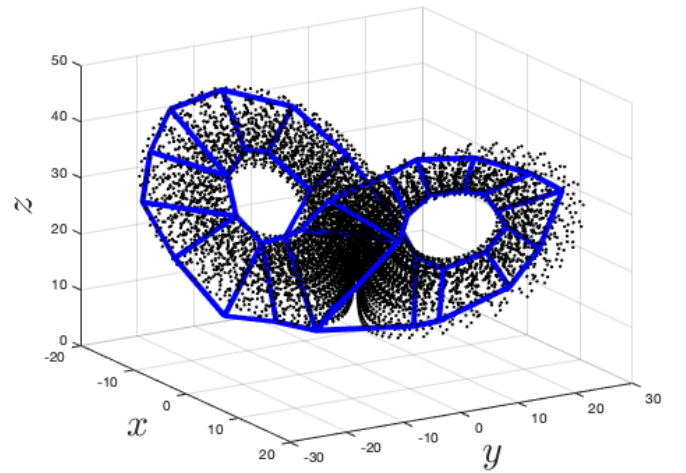


FIG. 1: Point cloud juxtaposed on the cell complex (blue lines) obtained by BraMAH for the deterministic Lorenz [22] attractor, with $\sigma = 0$ in Eq. (1).

here $r = 28$, $s = 10$, $b = 8/3$ are the standard parameter values for chaotic behavior.

The time-dependent sample measures μ_t associated with the SLM system (1) are probability measures for the population density of any ensemble of initial data driven by the same noise realization until time t , after removal of the transient behavior. Mathematically, these measures are of Sinai-Ruelle-Bowen (SRB) type [11, 30, 31], i.e. supported by the foliation of unstable manifolds that structure the random attractor [12].

A numerical estimation $\hat{\mu}_t$ of such a measure can be computed at any time instant t by a pullback approach, i.e. by letting a large set of N_0 initial points $\{(x_j, y_j, z_j)(t = 0) : j = 1, \dots, N_0\}$ “flow” in phase space from the remote past until time t , for a fixed noise realization ω . The convergence of the sample measure's approximation $\hat{\mu}_t = \hat{\mu}_t(N_0)$ is studied as the number N_0 of initial points increases; it is observed herein for $N_0 \simeq 10^8$.

Each point within a single point cloud at time t is mapped to a value of $\hat{\mu}_t$ that is obtained by averaging over a volume surrounding that point: higher or lower $\hat{\mu}_t$ -values correspond to more or less populated regions of the random attractor. We are interested in characterizing the topology of the point cloud's most populated regions but also in ascertaining this topology's robustness and persistence as N_0 changes. In order to do this, a threshold \bar{n} for $\hat{\mu}_t$ must be selected, as discussed later.

BraMAH computes the topology of a point cloud by assuming that points are locally distributed around a branched manifold. This allows one to approximate locally sets of points by m -disks, where m is the manifold's local dimension, and $m = 2$ in the case at hand.

The points in the cloud are thus classified by “patch decomposition” into locally defined patches of points. This procedure ensures that each patch has points in common with the neighboring ones, in order to keep track of the gluing prescriptions between them. Next, each patch will be associated with an n -cell.

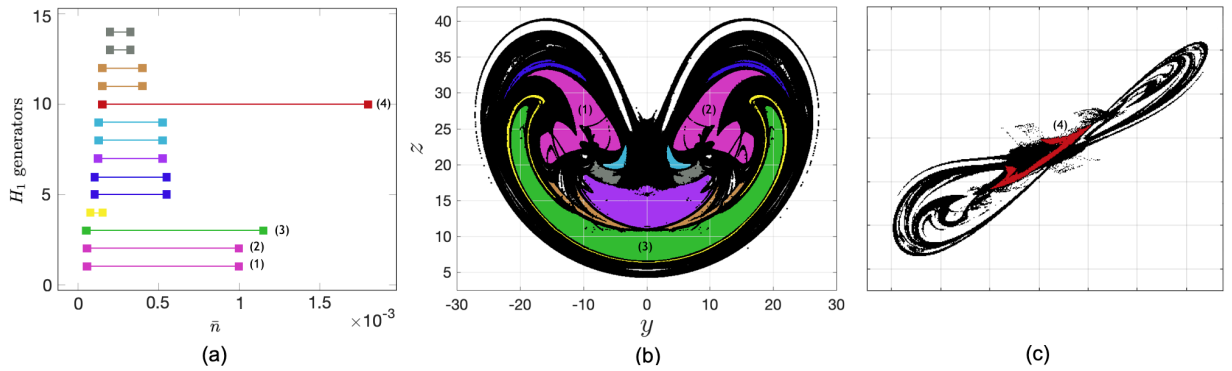


FIG. 2: LORA snapshot at $t = 40.27$, for $\sigma = 0.3$. (a) lifetime of the 1-holes as the density threshold \bar{n} is increased; the longest-lived ones are labeled with numbers (1)–(4); (b) (y, z) projection of the filtered point cloud ($\bar{n} = 2 \times 10^{-4}$) with 13 colored 1-holes; (c) projection onto the plane $-2.25x - 20y + 6z = 0$ of the filtered point cloud with the 1-hole labeled (4) in red.

An n -cell is a set that is mapped through a continuous invertible map into the interior of an n -disk, with boundaries divided into a finite number of lower-dimensional cells, called faces. A cell complex \mathbb{K}_h of dimension h is a finite set of cells, such that their faces are elements of the complex, the interiors of no two cells intersect, and the highest dimensional cell is an h -cell.

The topological properties of a cell complex \mathbb{K}_h are expressed in terms of its homology groups $\{\mathbb{H}_k : k = 0, \dots, h\}$. A k -chain is a linear combination of k -cells with integer coefficients. The algebra of these chains allows for a description of the connectivity of the cells at each k -level. A k -hole is a closed chain, called a k -cycle, that is not the border of any higher-dimensional cell.

In order to compute the H_k groups, BraMAH builds a boundary matrix with the borders of the cells to determine which k -cycles are homologous to others. The k -cycles that are homologically independent are appended to H_k . The output is a set of homology groups H_k spelled out in terms of their generators.

III. RESULTS

To start our study, we provide first a BraMAH analysis of the classical Lorenz [22] attractor, with $\sigma = 0$ in Eq. (1). The strange attractor and the cell complex associated with its 2-dimensional branched manifold is shown in Figure 1. The cell complex presents one connected component, i.e. $H_0 \sim \mathbb{Z}$, two homologically independent 1-holes associated with each wing of the butterfly, i.e. $H_1 \sim \mathbb{Z}^2$, and no enclosed cavities, i.e. $H_2 \sim \emptyset$.

Generating point clouds associated with solutions of the SLM yields data sets in the form of 3-dimensional point clouds of $N_0 = 10^8$ points. These point clouds are filtered, and the points in the filtered point cloud correspond to μ_t values greater than a threshold value \bar{n} . These filtered point clouds are used to construct cell complexes at each \bar{n} value using the BraMAH method.

In Figure 2, LORA is computed at time $t = 40.27$ with noise intensity $\sigma = 0.3$. The barplot in panel (a) shows the lifetime of 1-holes — i.e., of H_1 generators — as the

density threshold \bar{n} is increased: each bar starts at the first \bar{n} -value where the 1-hole appears, and ends at the \bar{n} where it disappears. Notice that, at this t -value, there are only four 1-holes that are “long-lived” as the value \bar{n} of the threshold increases.

The filtered point cloud is constructed using $\bar{n} = 2 \times 10^{-4}$ as threshold value for the approximated sample measure $\hat{\mu}_t$: Figure 2(b) shows the projection of the filtered point cloud onto the (y, z) -plane, with thirteen 1-holes colored and three of them labeled with the numbers (1), (2) and (3). Panel (c) shows a 3-dimensional view of the filtered point cloud with the persistent 1-hole labeled with number (4) in red. The colors of the holes correspond to those of the bars in the barplot of Fig. 2(a). In this work, we analyze the topology of successive LORA snapshots with noise intensity $\sigma = 0.3$.

The local dimension of the branched manifold remains the same as in the deterministic case: LORA is thus a locally 2-dimensional branched manifold. Noise adds neither connected components nor cavities to the manifold, so that the groups $H_0 \sim \mathbb{Z}$ and $H_2 \sim \emptyset$ are the same as in Figure 1. The topological distinctions between LORA and the classical strange attractor of Lorenz [22] are thus stored by H_1 . One notices that the number of 1-holes changes from one snapshot to another, with holes created or destroyed by the noise in the course of time.

This situation is illustrated in Figure 3 for 3 successive snapshots, at $t = 40.09, 40.18$ and 40.27 ; for each snapshot, we selected a threshold value \bar{n} at which the most persistent 1-holes occur. The filtered point clouds are given in the 3 top panels, while the corresponding cell complexes are presented in the 3 bottom panels. The number of 1-holes undergoes large changes from one snapshot to the next, as suggested by the video of LORA in the Supplementary Material of Chekroun et al. [12].

IV. CONCLUSION

We have presented here a topological analysis of a paradigmatic random attractor associated with the Lorenz convection model. The branched manifold we

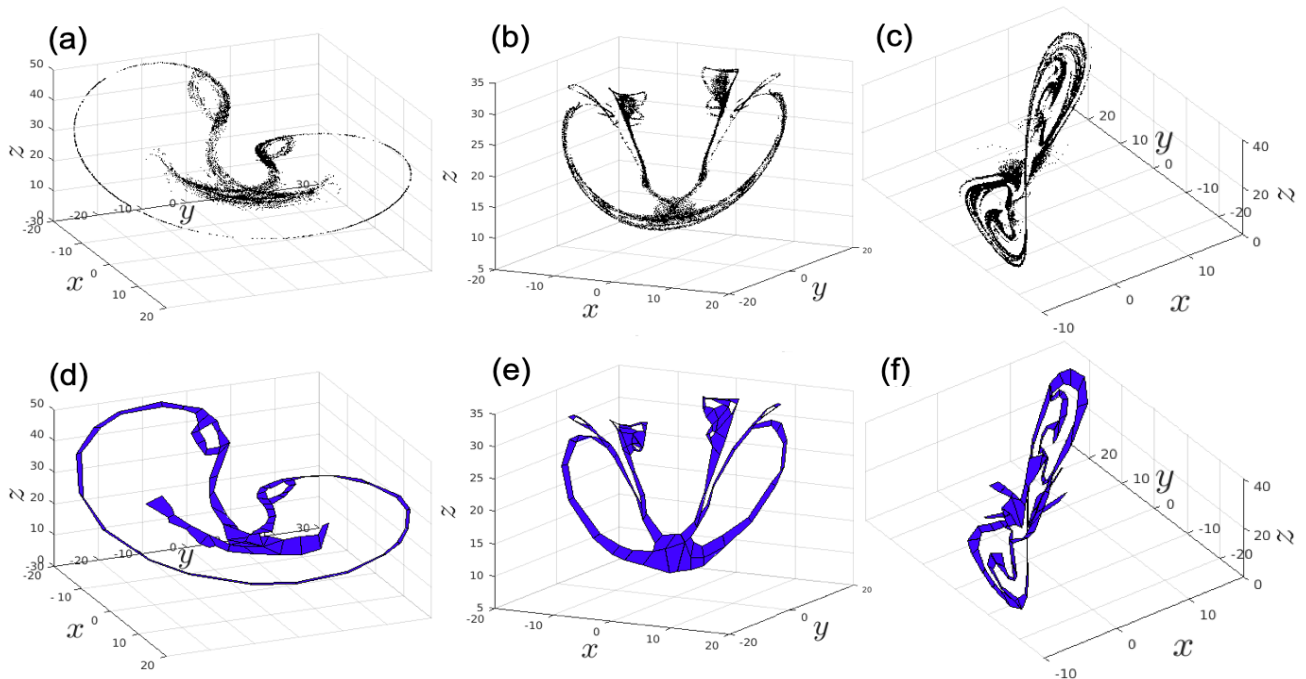


FIG. 3: Two representations of LORA snapshots with $\sigma = 0.3$ and $N_0 = 10^8$: filtered point clouds (a)–(c) and cell complexes (d)–(f). (a,d) $t = 40.09$, $\bar{n} = 6 \times 10^{-4}$, $H_1 \sim \mathbb{Z}^3$; (b,e) $t = 40.18$, $\bar{n} = 2.25 \times 10^{-3}$, $H_1 \sim \mathbb{Z}^{10}$; and (c,f) $t = 40.27$, $\bar{n} = 7 \times 10^{-4}$, $H_1 \sim \mathbb{Z}^4$.

constructed provides a coarse skeleton of this attractor.

Our study shows a marked difference between the unperturbed and the noise-driven cases. The stochastically perturbed system's random attractor, dubbed LORA, presents a much richer structure than the deterministic strange attractor, with a topology that also changes drastically in time. We believe that the framework introduced in this article to characterize such changes in topological features offers promising perspectives for the understanding of topological tipping points in general.

ACKNOWLEDGMENTS

This work is supported by the MATH-GEO (18-MATH-04) project of the Regional Program MATH-AmSud (D.S.). G.D.C. gratefully acknowledges support of her postdoctoral scholarship from CONICET. M.D.C.'s work has been partially supported by the European Research Council (ERC) under the European Union's Horizon 2020 research and innovation program (Grant Agreement No. 810370). The article is TiPES contribution #46; this project has received funding from the European Union's Horizon 2020 research and innovation program under grant agreement No. 820970 (M.G.)

APPENDIX A: PULLBACK ATTRACTORS

Consider a nonautonomous dynamical system (NDS),

$$\dot{x} = F(t, x); \quad (2)$$

here $F : \mathbb{T} \times X \rightarrow X$ governs the evolution of the state $x \in X$, \mathbb{T} can be the field \mathbb{R} or \mathbb{N} , and X is a complete metric phase space. The case of $\mathbb{T} = \mathbb{R}$ corresponds to a flow in continuous time, while $\mathbb{T} = \mathbb{N}$ corresponds to a map in discrete time.

Let $\Phi : \mathbb{T} \times \mathbb{T} \times X \rightarrow X$ be a mapping, where $\Phi(t, s, x) = x(t) \forall t \geq s$, is the solution to (2) at time t with initial state $\Phi(s, t_0, x) = x_0$. The map Φ provides a two-parameter description of the system's evolution in $(s, t) \in \mathbb{T}^2$, while in autonomous systems, due to the invariance $\Phi(s, t) = \Phi(t - s) \forall t \geq s$, a single parameter $t \in \mathbb{T}$ suffices to describe this evolution.

In the case of forced and dissipative systems, one can define a collection of subsets called a *pullback attractor* (PBA) [6, 7, 12, 32].

Definition 1 A PBA is a family $\bigcup_{t \in \mathbb{T}} \mathcal{A}(t)$, where $\mathcal{A}(t)$ is a compact subset of X at each time t . For each $t \in \mathbb{T}$, this family has two fundamental properties:

$$(1) \Phi(s, t, \mathcal{A}(t)) = \mathcal{A}(t), \forall s \leq t;$$

$$(2) \lim_{s \rightarrow -\infty} d(\Phi(s, t, B), \mathcal{A}(t)) = 0 \forall B \in X, \text{ where } d \text{ is the Hausdorff semi-distance.}$$

According to (1) and (2) above, the family $\mathcal{A}(t)$ is invariant under the system's dynamics and it attracts at each time t all compact initial subsets B from the remote past; see also Ghil et al. [7, Fig. A.1] for a simple illustration.

APPENDIX B: RANDOM DYNAMICAL SYSTEMS

In physical systems, such as those encountered in the climate sciences, random time-dependent forcing is often present [4]. When that is so, it becomes necessary to model this type of systems using stochastic differential equations [6].

In the theory of random dynamical systems (RDSs), random PBAs are known as random attractors and they can be constructed in an extended phase space composed of the phase space X and a probability space. A probability space $(\Omega, \mathcal{F}, \mathbb{P})$ is a three-tuple, where Ω is the sample space; \mathcal{F} is the event space, formulated as a σ -algebra; and $\mathbb{P} : \mathcal{F} \rightarrow [0, 1]$ is the probability function.

A model of the noise $\theta_t : \Omega \rightarrow \Omega$ for all times t enables one to associate the state $\omega \in \Omega$ at initial time $t = 0$ with its state after a time t has elapsed. This model θ_t is called the driving system and one sets $\theta_0(\omega) = \omega$ [7].

A mapping $\varphi : \mathbb{T} \times \Omega \times X \rightarrow X$ has the cocycle property when $\varphi(t, \omega) := \varphi(t, \omega, \cdot) : X \rightarrow X$ satisfies the following conditions [6]:

- (i) $\varphi(0, \omega) = id_X, \forall \omega \in \Omega$.
- (ii) $\varphi(t + s, \omega) = \varphi(t, \theta_s(\omega)) \circ \varphi(s, \omega) \forall s, t \in \mathbb{T}$ and $\omega \in \Omega$.

Property (i) just sets the initial state of the cocycle, while property (ii) can be formulated in simple words as stating that a cocycle is time invariant in the sense that going from a copy of X at time 0 to one at time s and from there to one at time $t + s$ is the same as going directly from 0 to $t + s$; see also Ghil et al. [7, Fig. A.2].

Definition 2 A mapping φ with the cocycle property on a measurable space (X, \mathcal{B}) , with \mathcal{B} a σ -algebra, is called a measurable RDS over $(\Omega, \mathcal{F}, \mathbb{P}, \theta_t)$.

The evolution of a stochastic system can be thus modeled by a measurable RDS and the concept of a random attractor, $\bigcup_{t \in \mathbb{T}} \mathcal{A}(t; \omega)$, can be seen as an extension of a PBA. In the RDS case, however, each individual “random PBA” depends on the specific realization $\omega \in \Omega$ of the noise. The resulting family of random compact sets $\bigcup_{\omega \in \Omega} \mathcal{A}(\omega)$ provides a complete description of all the possible states of the system that are likely to be observed at time t .

APPENDIX C: INVARIANT MEASURES

The dynamics on many attractors can be described by a probability measure, which “counts” how frequently the attractor’s subsets are visited by the dynamics (2).

Given a measurable function f , a measure μ is called invariant under f if, for every measurable set $C \in \mathcal{B}$, $\mu(f^{-1}(C)) = \mu(C)$. A class of invariant measures of interest are Sinai-Ruelle-Bowen (SRB) measures [11, 30, 31].

In the RDS context, the invariant measure μ is defined on the product space $\Omega \times X$ and the invariance is with respect to the skew product $\Theta := (\varphi, \theta)$.

Definition 3 Given a measurable RDS φ over θ , a measure μ on $(\Omega \times X, \mathcal{F} \otimes \mathcal{B})$ is called an invariant measure for φ if it satisfies:

- (i) $\Theta(t)\mu = \mu, \forall t \in \mathbb{T}$
- (ii) $\pi_\Omega \mu = \mu$, where $\pi_\Omega : \Omega \times X \rightarrow \Omega, \pi_\Omega(\omega, x) = \omega$.

The projection π onto Ω satisfies $\pi_\Omega \circ \Theta(\cdot) = \theta \circ \pi_\Omega$, and it follows that $\forall t \in \mathbb{T}, \pi_\Omega \mu = \theta_t(\pi_\Omega \mu)$.

Note that, if invariant measures μ of a given RDS exist, they lift the probability measure \mathbb{P} from (Ω, \mathcal{F}) to $(\Omega \times X, \mathcal{F} \otimes \mathcal{B})$.

Definition 4 A function $\mu_\omega(\cdot) : \Omega \times \mathcal{B} \rightarrow [0, 1]$ is called a sample measure of μ with respect to \mathbb{P} if it satisfies:

- (1) For each $B \in \mathcal{B}$, μ_ω is \mathcal{F} -measurable,
- (2) μ_ω is a probability measure on (X, \mathcal{B}) for almost all $x \in X$ with respect to \mathbb{P} ,
- (3) For all $A \in \mathcal{F} \otimes \mathcal{B}$

$$\mu(A) = \int_\Omega \int_X 1_A(\omega, x) \mu_\omega(dx) \mathbb{P}(d\omega),$$

$$i.e., \mu(d\omega, dx) = \mu_\omega(dx) \mathbb{P}(d\omega)$$

Let \mathcal{A} be a random attractor: it supports all the invariant measures and $\mu(\mathcal{A}) = 1 \Leftrightarrow \mu_\omega(\mathcal{A}(\omega)) = 1$ means that each sample of \mathcal{A} supports the sample measure μ_ω . For a realization ω , $\mathcal{A}(t; \omega)$ determines the destination at time t of the regions that are affected by the RDS.

An essential feature that a sample measure μ_ω supported by the attractor must possess is that it shed light on the spatio-temporal distribution of the attractor’s properties according to probabilities given by μ_ω . In particular, physical measures are sample measures that meet this condition [30]. Chekroun et al. [12, Appendix C] have proven rigorously that LORA supports an SRB measure and shown by very careful numerical computations that it is physical, too.

For clarity, recall that an SRB measure μ — subject to certain technical conditions — is physical in the following, more precise sense; namely, that for any continuous observable $\psi : X \rightarrow \mathbb{R}$, the time average equals the ensemble average for almost all initial data x_0 , with respect to the usual, Lebesgue measure, where $x_0 \in B_\mu$ and B_μ is the basin of attraction of μ ; see Chekroun et al. [12, Eq. (5)]. A technical condition that is relatively easy to check is that the linearization of the cocycle $\varphi(t, \omega, x)$ at x must have a positive Lyapunov exponent for μ -almost every x ; this condition implies that the system is chaotic. For the other sufficient conditions, please see Chekroun et al. [12, Appendix C].

Note that the existence of an SRB measure μ does not guarantee its uniqueness, and that two such measures

$\mu \neq \nu$ may also have different attractor sets $B_\mu \neq B_\nu$. The extensive numerical calculations in [12] and herein have given no indication, though, of another SRB mea-

sure being present, but the uniqueness of LORA's SRB, and hence physical, measure has not been proved rigorously, to the best of the authors' knowledge.

-
- [1] M. Ghil et al., Rev. Geophys. **40**, RG000092 (2002).
- [2] C.-P. Chang et al., *Climate Change: Multidecadal and Beyond* (World Scientific, 2015).
- [3] M. Ghil, Earth and Space Science **6**, 1007 (2019).
- [4] M. Ghil and V. Lucarini, Rev. Mod. Phys. **92**, 035002 (2020).
- [5] P. E. Kloeden and M. Rasmussen, *Nonautonomous Dynamical Systems* (American Meteorological Society, 2011).
- [6] L. Arnold, *Random Dynamical Systems* (Springer, 1988).
- [7] M. Ghil, M. D. Chekroun, and E. Simonnet, Phys. D **237**, 2111 (2008).
- [8] M. Gladwell, *The Tipping Point: How Little Things Can Make a Big Difference* (Little, Brown, 2006).
- [9] M. D. Chekroun, M. Ghil, and J. D. Neelin, in *Adv. Nonlin. Geophys.*, edited by A. Tsonis (Springer Science & Business Media, 2018), pp. 1–33.
- [10] F. Ledrappier and L.-S. Young, Probab. Theory Related Fields **80**, 217 (1988).
- [11] L.-S. Young, J. Stat. Phys. **166**, 494 (2017).
- [12] M. D. Chekroun, E. Simonnet, and M. Ghil, Phys. D **240**, 1685 (2011).
- [13] H. Poincaré, J. Èc. polythec. Mat. **1**, 1 (1985).
- [14] A. Hatcher, *Algebraic Topology* (Cambridge University Press, 2002).
- [15] M. R. Muldoon et al., Phys. D **65**, 1 (1993).
- [16] D. Sciamarella and G. B. Mindlin, Phys. Rev. Lett. **82**, 1450 (1999).
- [17] D. Sciamarella and G. B. Mindlin, Phys. Rev. E **64**, 036209 (2001).
- [18] R. Gilmore, Rev. Mod. Phys. **4**, 1455 (1998).
- [19] J. Birman and R. F. Williams, Topology **22**, 47 (1983).
- [20] P. Holmes and R. F. Williams, Arch. Ratio. Mech. Anal. **90**, 115 (1985).
- [21] G. M. Mindlin and R. Gilmore, Phys. D **58**, 229 (1992).
- [22] E. N. Lorenz, J. Atmos. Sci. **20**, 130 (1963).
- [23] G. D. Charó, G. Artana, and D. Sciamarella, Phys. D **405**, 132371 (2020).
- [24] L. C. Kinsey, *Topology of Surfaces* (Springer, 1997).
- [25] H. Edelsbrunner and J. Harer, Contemp. Math. **453**, 257 (2008).
- [26] G. Carlsson, Acta Num. **23**, 289 (2014).
- [27] F. Chazal and M. Bertrand, arXiv:1710.04019 (2017).
- [28] F. J. Romeiras, C. Grebogi, and E. Ott, Phys. Rev. A **41**, 784 (1990).
- [29] G. Drótos, T. Bódai, and T. Tél, J. Climate **28**, 3275 (2015).
- [30] J.-P. Eckmann and D. Ruelle, Rev. Mod. Phys. **57**, 617 (1985).
- [31] L.-S. Young, J. Stat. Phys. **108**, 733 (2002).
- [32] T. Caravallo, G. Łukaszewicz, and J. Real, Nonlinear Anal. **64**, 484 (2006).